Field characterization of therapeutic ultrasound phased arrays through forward and backward planar projection

G. T. Clement and Kullervo Hynynen
Brigham & Women's Hospital, Harvard Medical School, 75 Francis Street, Boston, Massachusetts 02115

(Received 30 August 1999; accepted for publication 27 March 2000)

Spatial planar projection techniques propagate field measurements from a single plane in front of a transmitter to arbitrary new planes closer to or further away from the source. A linear wave vector frequency-domain projection algorithm is applied to the acoustic fields measured from several focused transducer arrays designed for ultrasound therapy. A polyvinylidene difluoride hydrophone is first scanned in a water tank over a plane using a three-dimensional positioning system to measure the complex pressure field as a function of position. The field is then projected to a series of new planes using the algorithm. Results of the projected fields are compared with direct measurements taken at corresponding distances. Excellent correlation is found between the projected and measured data. The method is shown to be accurate for use with phase-controlled field patterns, providing a rapid and accurate method for obtaining field information over a large spatial volume. This method can significantly simplify the characterization procedure required for phased-array application used for therapy. Most significantly, the wavefront propagated back to a phased array can be used to predict the field produced by different phase and amplitude settings of the array elements. A field back-projected to the source could be used as an improved source function in acoustic modeling.
 [S0001-4966(00)01207-8]

PACS numbers: 43.80.Vj, 43.35.Yb [FD]

INTRODUCTION

Measurement of a radiating field across an appreciable spatial volume can require an exhaustive amount of physical measurement. However, knowledge of the field over these volumes may be necessary when the source involves complicated amplitude and phase shading, since the field resulting from the response of a physical transducer can be difficult to predict. Spatial planar propagation methods[1] greatly reduce the data required for global reconstruction of a linear field. These methods allow the acoustic pressure in a single plane in front of a source to be rapidly propagated to arbitrary new planes. This ability is particularly appealing for the case of therapeutic ultrasound arrays,[2–4] which use areas of high pressure to necrose cells through elevated temperature[5] or cavitation.[6] A full knowledge of the spatial field obtained from projected data could provide an accurate mapping of a focal region as well as identify unexpected intense sidelobes and other regions of high acoustic intensity away from the area of ultrasound treatment. Additionally, a pressure field projected to a plane near the transducer surface could provide information for precise field modeling.[7–9] Phased arrays consisting of a large number of elements could use the projected information to adjust the amplitude and phase of individual driving signals and improve radiated signals.

A variety of harmonic and transient planar propagation algorithms has been described. These algorithms generally relate the fields of two planes in terms of a transfer function in either the wave vector-frequency[10] domain or the wave vector-time domain.[11] Experimental harmonic[12,13] and transient[10] fields for a number of transducer geometries have been propagated using these approaches. The present study examines the use of forward and backward projection for the characterization and analysis of the fields produced by therapeutic phased arrays. We utilize the 2D angular spectrum method[1] for projecting harmonic waves. The algorithm is valid in a boundless, lossless region. Basic theory is outlined in Sec. I for the case of a linear, freely propagating field. In this limit, the field may be propagated to any plane that does not intersect with the source. Spherically concave transducers considered here may be propagated backward to the plane tangent to the edge of the transducer.

To evaluate the method for the case of phased arrays, phase-controlled field patterns described in Sec. II are produced by three transducer arrays with varying geometric configurations. Each of these transducers and their corresponding field patterns are designed for use in a variety of therapeutic applications. A single planar scan is performed using a stepping motor-controlled positioning system to scan a polyvinylidene difluoride (PVDF) hydrophone over an arbitrary plane situated normal to the acoustic axis of propagation. The fast Fourier transform (FFT)-based algorithm then propagates the field to a series of new planes, both in the acoustic near field and far field. In Sec. III, the projections are compared with experimental measurements of the planes corresponding to the experimental distances. Results indicate that the projected fields correlate closely with directly measured fields.

I. THEORY

The projection algorithm assumes that the acoustic field satisfies the linearized acoustic wave equation. While therapeutic arrays generally operate at high powers, the linear approximation is found to be appropriate for evaluating transducers.[14] For a time-harmonic field, the temporal depen-

dence can be separated so that the pressure is expressed as $P(r,t)=\tilde{P}(r)e^{i\omega t}$, and the wave equation becomes

$$\left(\nabla^2+\frac{\omega^2}{c^2}\right)\tilde{P}(r)=0, \tag{1}$$

where c is the speed of sound and ω is the angular frequency. A Helmholtz equation in Cartesian coordinates is obtained through the substitution of the 2D Fourier integral

$$\tilde{P}(x,y,z)=\frac{1}{2\pi}\int\int \tilde{p}(k,k,z)e^{i\omega t}e^{ik_x x}e^{ik_y y}\,dk_x\,dk_y \tag{2}$$

into Eq. (1) yielding

$$\frac{\partial\tilde{p}(k_x,k_y,z)}{\partial z}+\left(\frac{\omega^2}{c^2}-k_x^2-k_y^2\right)\tilde{p}(k_x,k_y,z)=0. \tag{3}$$

To propagate the field in a plane at a distance z_0 in front of a source to a new plane z, the advanced solution of Eq. (3) is used

$$\tilde{p}(k_x,k_y,z)=\tilde{p}(k_x,k_y,z_0)e^{i(z-z_0)\sqrt{(\omega^2/c^2)-k_x^2-k_z^2}}. \tag{4}$$

In wave vector space, the field recorded in a plane z_0 is thus related to the field at any other plane z by a simple transfer function given in the right-hand side of Eq. (4). The pressure field in space at z may be obtained by taking the inverse Fourier transform of Eq. (4).

Backward projection to the source could serve as an source function for more realistic acoustic modeling. The source function can also be numerically adjusted to predict the field for additional field patterns.[15] This process is demonstrated in a simple example where a field is backward projected toward the source and numerically modified with a synthetic phase pattern. The adjusted field is then projected away from the source. This projected field is found to closely correlate with hydrophone measurements when the transducer is driven with the new phase pattern.

II. MATERIALS AND METHODS

A. Apparatus

All experiments were performed in a water tank, depicted in Fig. 1. The inner walls of the tank were covered with rubber to prevent reflection and standing wave interference. A transducer (T) was rigidly mounted with its axes of propagation parallel with the long axis of the tank. A Precision Acoustics 0.5-mm PVDF hydrophone (H) was attached to a Parker 3D stepping motor-guided positioning system and scanned over the plane perpendicular to the acoustic axis. The hydrophone signal was amplified by a Precision Acoustics submersible preamplifier (PA) and recorded by a Tektronix TDS 380 oscilloscope (O). The hydrophone position and data acquisition were both computer controlled (C).

Three transducers, described in detail below, were used for the experiments. Each of the arrays consisted of fully isolated air-backed PZT elements. Each array in the study was powered by a phased-array driving system (DS) manufactured in-house, and equipped with power and phase feedback for increased control.[16] Individual channels of the arrays were equipped with impedance matching circuitry,

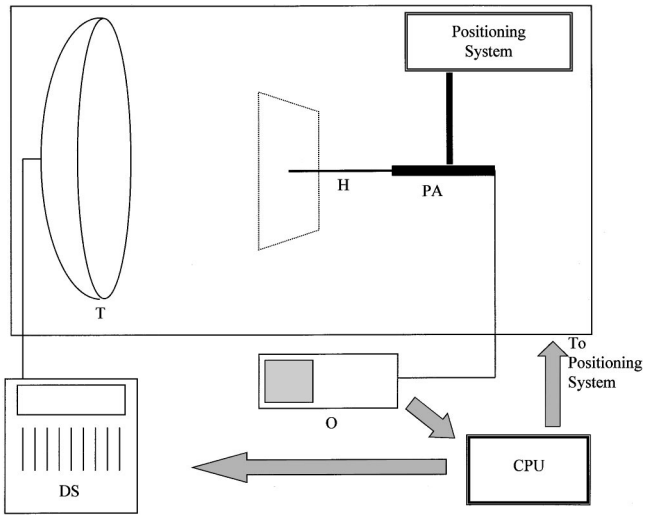

FIG. 1. Experimental setup for driving phased arrays and measuring the acoustic signal.

matching the channel to electrical resonance at 50 Ω, to assure maximum power output to the transducer. To accommodate the hydrophone in the focal region, all experiments were performed at low power, with total electrical inputs not exceeding 1 W.

In each experiment the hydrophone was scanned over a plane 10×10 mm^2 at steps of 0.4 mm and resulting in a sampling resolution of 2.5 pts/mm^2. While the hydrophone is not omnidirectional, the directivity of the hydrophone is nearly constant over the measured planes. A sensitivity drop of no less than -0.7 dB is expected for the frequencies and angles encountered in the planar measurements. For each sampled position, the time trace recorded by the oscilloscope was downloaded to a PC and Fourier transformed to obtain the amplitude and phase at the driving frequency of the transducer. Fields were measured in the planes at the geometric focus and 10 mm in front and behind the focus so that they could be compared with projected data. Additionally, a line scan was performed along the axis of propagation using the Parker positioning system. Data from the focal plane were then entered into the projection algorithm based on the relation described in Eq. (4) and propagated. The algorithm typically took less than 5 s to complete the projection using a 250-MHz Pentium processor with 128 MB of RAM.

A quantitative comparison of the measured and projected planes is performed using a rms measurement calculated for the difference in the amplitudes

$$R=\left[\frac{\Sigma_{i,j}^{M,N}(P_{ij}-P'_{ij})^2}{\Sigma_{i,j}^{M,N}(P_{ij})^2}\right]^{1/2}, \tag{5}$$

where P_{ij} is a measured amplitude point over an $M\times N$ matrix and P'_{ij} is an element of the projection.

B. Transducers

The first transducer considered is a 1.5-MHz 14-element concentric ring array[17] with both a diameter and radius of curvature of 100 mm, as shown in Fig. 2(a). The rings are all equal in width as measured perpendicular to the radial axis. The ultrasound focus is steered away from the geometric

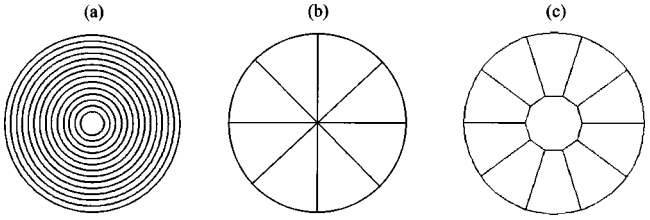

FIG. 2. Overhead view of focused phased arrays used in the study. (a) 14-element concentric ring array. (b) Eight-element sector vortex array. (c) A ten-sided center element with adjacent outer elements.

point of convergence by setting the contribution of individual elements in phase at the desired focal point. The transducer was operated with the focus shifted from 100 to 90 mm. Power to the elements was adjusted according to the ring surface area so that the intensity is uniform across the transducer.

The second array is an eight-element sector vortex array,[18] 1.1-MHz array with diameter of 100 mm and an 80-mm radius of curvature, depicted in Fig. 2(b). A sector vortex array consists of N symmetrical elements such that N is an even power of 2. The array can be driven to produce $N/2$ different acoustic field patterns by phase shifting. The phases for the elements of a sector vortex array are calculated as follows:

$$\theta_n = m \cdot n\left(\frac{2\pi}{N}\right), \tag{6}$$

where θ_n is the phase of element $n=0,1,...,N-1$, and $m \leqslant N/2$ is the mode of phase revolution. For the experiment the array was powered in modes zero and four.

The third array is an 11-element 0.67-MHz transducer with a diameter of 100 mm and a radius of curvature equal to 80 mm. The geometric configuration of the elements is shown in Fig. 2(c). Each of the elements in this array is driven in phase; however, the resulting field pattern presented differ from that of a uniform transducer due to uneven displacement across the elements.

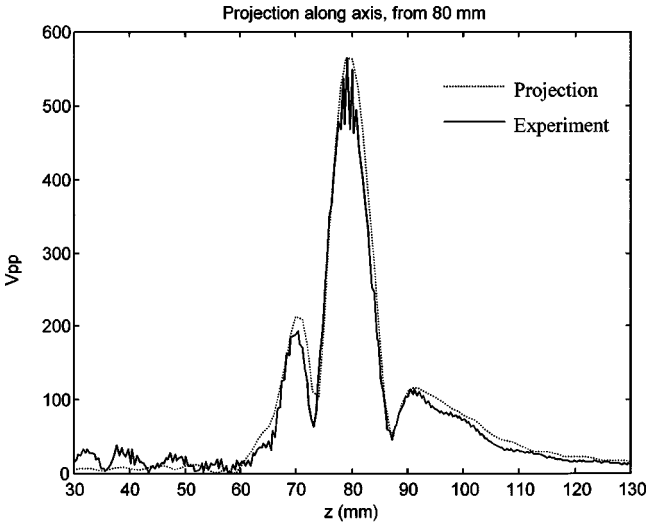

FIG. 4. The measured (solid) and projected (dotted) signals along the axis of propagation due to the sector vortex array driven in mode 0. Projections are from the plane at $z=80$ mm.

III. RESULTS

The sector vortex transducer in mode 0 was scanned over planes at distances of 65, 80, and 90 mm from the transducer face as shown in Fig. 3(a). Data along the plane at 80 mm [Fig. 3(a 2)] was entered into the projection algorithm and propagated to distances corresponding to the three measured planes, as displayed in Fig. 3(b). The 80-mm data in Fig. 3(b 1) simply represent a projected distance of 0 mm and serve to check the algorithm. Next, a line along the axis of propagation was measured between 30 and 130 mm from the transducer. The 80-mm planar data set was then projected over this line. The measured and projected data are displayed

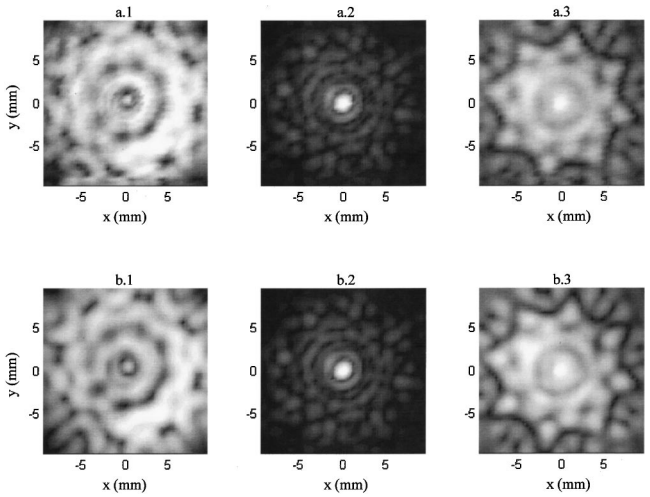

FIG. 3. (a) Radial measurements of the sector vortex array in mode 0, and (b) their corresponding projections. Image intensity is linearly scaled with the acoustic pressure amplitude. Fields are measured at distances of (a 1) 70 mm, (a 2) 80 mm, and (a 3) 90 mm form the source. Projection from $z=80$ mm to distances of (b 1) 70 mm, (b 2) 80 mm, and (b 3) 90 mm.

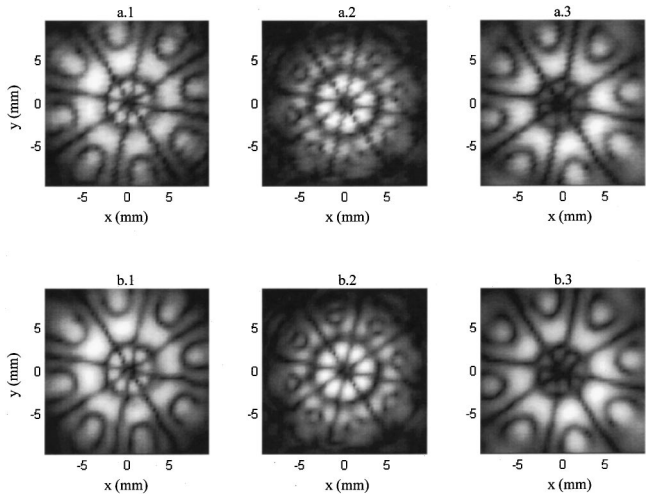

FIG. 5. (a) Radial measurements of the sector vortex array in mode 4, and (b) their corresponding projections. Image intensity is linearly scaled with the acoustic pressure amplitude. Fields are measured at distances of (a 1) 70 mm, (a 2) 80 mm, and (a 3) 90 mm from the source. Projection from $z=80$ mm to distances of (b 1) 70 mm, (b 2) 80 mm, and (b 3) 90 mm.

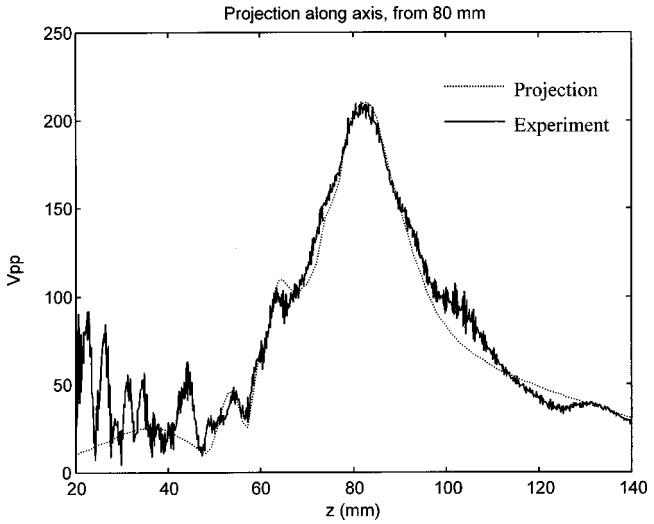

FIG. 6. The measured (solid) and projected (dotted) signals along the axis of propagation due to the concentric ring array focused at 80 mm. Projections are from the plane at $z=90$ mm.

in Fig. 4. The mean deviation across the line is 3% of the signal peak, with a maximum deviation of 20% occurring in the region close to the transducer.

The rms comparison given in Eq. (5) yielded values of 5.0% at 65 mm, 0.3% at 80 mm, and 0.6% at 90 mm. Next, the sector vortex transducer was operated in mode 4 and measurements were made in planes similar to those scanned in mode 0. Experimental results displayed in Fig. 5(a) may be compared with the projections shown in Fig. 5(b). The mode 4 projection produced rms difference values of 2.4% at 65 mm, 0.4% at 80 mm, and 2.2% at 90 mm.

Planar scans of the concentric ring array were performed at distances of 70, 80, and 90 mm from the transducer. Projections were calculated with data from 90 mm. Discrepancies of 1.0%, 1.4%, and 0.2% were calculated using Eq. (5). As with the concentric ring array, axial measurements were acquired and compared with a projection using the 90-mm data. The result is shown in Fig. 6. A mean deviation 5% of

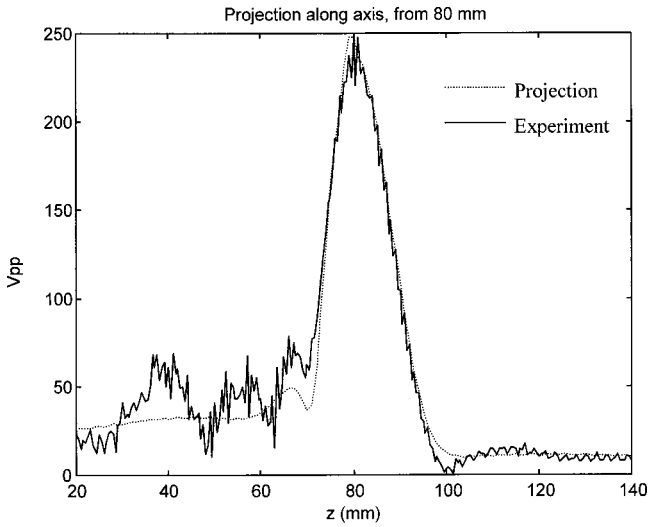

FIG. 7. The measured (solid) and projected (dotted) signals along the axis of propagation due to the 11-element array with all elements driven in phase. Projections are from the plane at $z=80$ mm.

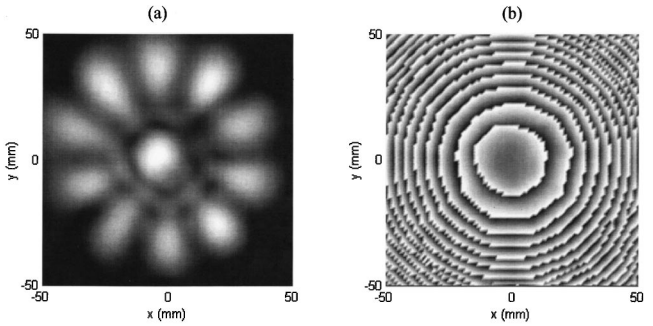

FIG. 8. Projection of the 11-element array's signal from 80 mm to the transducer. (a) A linear intensity plot of the acoustic pressure amplitude, and (b) the phase of the acoustic pressure.

the signal peak is found across the axis, with a maximum deviation of 30%.

The 11-element array was measured at 70, 80, and 90 mm. The associated rms discrepancies were 0.3%, 5%, and 0.6%, respectively. As with the sector vortex transducer, data from the 80-mm plane were projected. Results of the line scan are presented in Fig. 7, indicating a mean deviation of 4% of the maximum amplitude with a maximum deviation of 18%.

To illustrate the ability of the method to project toward the source, the acoustic field of the 11-element array is propagated close to the transducer face. In Fig. 8 the projection from 80 to 20 mm indicates that field information at the focus is sufficient to identify the radiation of the individual elements. The amplitude plot in Fig. 8(a) of this planar scan illustrates a lack of uniformity in amplitude across individual elements, while the phase plot in Fig 8(b) shows the expected radial phase shifting across the array. The sector vortex transducer driven in mode 4 was projected toward the transducer face, showing amplitude variation in Fig. 9(a) and phase variation in Fig. 9(b). For the case of large phased arrays, projections could be used to determine amplitude and phase corrections for each element, improving the overall ultrasound field.

Fields projected backward to the transducer could also provide computer models with more realistic source functions. This is demonstrated in the following: (i) The sector vortex field in mode 0 was measured near its focus [Fig. 3(a 2)]. (ii) The data were projected backward to the transducer ($z=17.6$ mm). (iii) A synthetic mode 4 planar phase

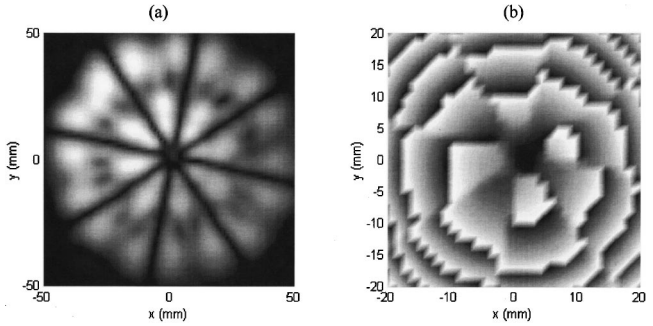

FIG. 9. Projection of the sector vortex mode 4 signal from 80 mm to the transducer. (a) A linear intensity plot of the acoustic pressure amplitude, and (b) the phase of the acoustic pressure.

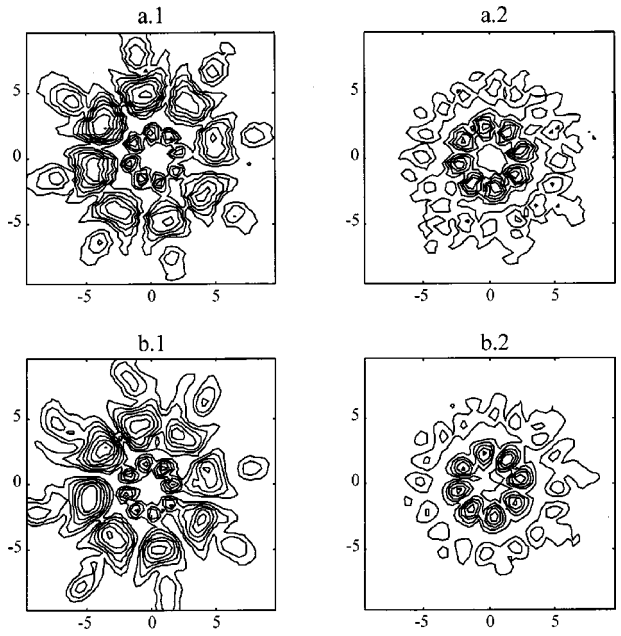

FIG. 10. Modeled mode 4 sector vortex field using mode 0 data projected from 80 mm to the transducer face, where a synthetic phase file is introduced. (a 1) Contour of the measured mode 4 field at 70 mm. (a 2) Contour of the measured mode 4 field at 80 mm. (b 1) The modeled field at 70 mm. (a 2) The modeled field at 80 mm. Contours lines are at 10% intervals of the signal amplitude.

file was generated and combined with the projected data. (iv) The new file was projected forward to 70 mm, resulting in the simulated field shown in Fig. 10(b 1). The field may be compared with the direct mode 4 measurement of Fig. 10(a 1). Similarly, the direct measurement and the corresponding modeled field at 80 mm are shown in Figs. 10(a 2) and 10(b 2).

IV. DISCUSSION

Projected fields presented in the previous section demonstrate excellent agreement with experimental measurement. An example of the algorithm's ability to reconstruct detailed lobe structure is seen in the amplitude values of the sector vortex mode 4 scan illustrated in Fig. 5(a). Looking along the radial direction, local maxima occurring before and after the signal peaks are found to be successfully reconstructed. Another feature apparent from comparing the experimental plots [Figs. 3(a) and 5(a)] with their projections [Figs. 3(b) and 5(b)] is the capacity of the algorithm to identify asymmetries in the field. The primary limitation to reconstruction of small features is the bandwidth of the spatial frequency. If required, the bandwidth could be increased by using a smaller hydrophone and increasing the sampling rate. It is stressed that the method assumes linear propagation through a homogeneous fluid and is limited to cases where this assumption holds.

A significant advantage of planar projection methods is their ability to identify asymmetries throughout the field from a single cross section of the field. Unexpected bias of the amplitude toward the fourth quadrant of the plane in Fig. 3(a 1) is also predicted by the backward projection of Fig. 3(b 1). Likewise, a peak in the second quadrant is predicted in the forward projection from 80 to 90 mm, Fig. 3(b 3), which also appears in the direct measurement, Fig. 3(a 3).

Planar projection allows fields to be calculated in areas that are normally difficult to measure, such as the high-intensity regions of a focused beam and at a distance close to the source where the hydrophone directionality can affect measurements. Although low-intensity ultrasound was used for the present experiment, the backward projection of the concentric ring array field into the focus could be performed for higher intensities, as long as the linear wave approximation is valid. Thus, a hydrophone designed for lower pressure fields could be used to predict a high-intensity focus. Discrepancy between the transducer and the hydrophone close to the source is observed in the axial scans shown in Figs. 6 and 7. The oscillations observed in the measured data may result from standing waves between the transducer and the hydrophone holder.

Projection of the field backward to the transducer could serve as a source function for a wide variety of modeling problems. Once propagated near the source, the original plane measured in a homogeneous medium can now be used as an accurate starting point in models that calculate fields through tissue and other heterogeneous layers. Further, from a single measurement the phase and amplitude of each element's response can be numerically adjusted to predict the field for additional field designs used for beam steering as well as multiple foci patterns.[15] This could be particularly useful in the case of arrays containing a large number of elements. The numeric phase shift presented in Fig. 10 demonstrates feasibility of numeric modification of the source function. In practice, large arrays may require several field patterns to be measured and projected to the surface in order to correctly adjust for element coupling.

V. SUMMARY

A linear planar projection algorithm was applied toward the projection of fields generated by focused phased arrays in water designed for therapeutic ultrasound. The algorithm provides a rapid and accurate method for characterizing a pressure field. Projection of a planar measurement to an arbitrary new plane takes under 5 s on a 250-MHz Pentium processor. Excellent correlation was observed between the projected data and direct measurements. The rms difference between the two planes was 5% or less for all distances considered. Further, the algorithm successfully identified peaks in the pressure amplitudes along the projected planes.

Several features of the algorithm are particularly appealing for use with focused therapeutic arrays. Direct measurements of the field in front of the transducer normally subject to interference can be projected backward from data near the focus where a much smaller area may be scanned. Field information near the face may be used for correction of the transducer driving signals. This information may also be used as a source function in conjunction with field modeling to be used for field control in heterogeneous tissues. In the case of high-intensity ultrasound, the focus of the transducer could be measured in a lower-intensity plane safe for a PVDF hydrophone and then projected into the converging

region. Finally, fast projection times allow asymmetries in the field or possible transducer defects to be quickly identified.

ACKNOWLEDGMENT

This work was supported by Grant No. CA 46627 from the National Institutes of Health.

[1] P. R. Stepanishen and K. C. Benjamin, ''Forward and backward projection of acoustic fields using FFT methods,'' J. Acoust. Soc. Am. **71**, 803–812 (1982).
[2] L. A. Frizzell, P. J. Benkeser, K. B. Ocheltree, and C. A. Cain, ''Ultrasound phased arrays for hyperthermia treatment,'' IEEE Ultrasonics Symp. **2**, 931–935 (1985).
[3] E. S. Ebbini and C. A. Cain, ''A spherical-section ultrasound phased array applicator for deep localized hyperthermia,'' IEEE Trans. Biomed. Eng. **38**(7), 634–643 (1991).
[4] D. R. Daum and K. Hynynen, ''Spherical phased array design optimized for ultrasound surgery,'' 1997 IEEE Ultrasonics Symposium Proceedings—An International Symposium, 1315 (1997).
[5] G. ter Haar, ''Therapeutic ultrasound,'' Eur. J. Ultrasound **9**(1), 3–9 (1999).
[6] F. J. Fry, N. T. Sanghvi, R. S. Foster, R. Bihrle, and C. Hennige, ''Ultrasound and microbubbles: their generation, detection and potential utilization in tissue and organ therapy—experimental,'' Ultrasound Med. Biol. **21**(9), 1227–1237 (1995)
[7] C. J. Vecchio and P. A. Lewin, ''Finite amplitude acoustic propagation modeling using the extended angular spectrum method,'' J. Acoust. Soc. Am. **95**, 2399–2408 (1994).
[8] X. Fan, E. Moros, and W. L. Straube, ''Acoustic field prediction for a single continuous-wave source using an equivalent phased array method,'' J. Acoust. Soc. Am. **102**, 2734–2741 (1997).
[9] X. Fan, E. Moros, and W. L. Straube, ''A concentric-ring equivalent phased array method to model fields of large axisymmetric ultrasound transducers,'' IEEE Trans. Ultrason. Ferroelectr. Freq. Control **46**(4), 830–841 (1999).
[10] G. T. Clement, R. Liu, S. V. Letcher, and P. R. Stepanishen ''Forward projection of transient signals obtained from a fiber-optic pressure sensor,'' J. Acoust. Soc. Am. **104**, 1266–1273 (1998).
[11] M. Forbes, S. V. Letcher, and P. R. Stepanishen, ''A wave vector, time-domain method of forward projecting time-dependent pressure fields,'' J. Acoust. Soc. Am. **90**, 2782–2793 (1991).
[12] R. Reibold and F. Holzer, ''Complete mapping of ultrasonic fields without the wavelength limit,'' Acustica **58**, 11–16 (1985).
[13] M. E. Schafer and P. A. Lewin, ''Transducer characterization using the angular spectrum approach,'' J. Acoust. Soc. Am. **85**, 2202–2214 (1989).
[14] K. Hynynen, ''The role of nonlinear ultrasound propagation during hyperthermia treatments,'' Med. Phys. **18**(6), 1156–1163 (1991).
[15] D. R. Daum and K. Hynynen, ''Theoretical design of a spherically sectioned phased array for ultrasound surgery of the liver,'' Eur. J. Ultrasound **9**(1), 61–69 (1999).
[16] D. R. Daum, M. T. Buchanan, T. Fjield, and K. Hynynen, ''Design and evaluation of a feedback based phased array system for ultrasound surgery,'' IEEE Trans. Ultrason. Ferroelectr. Freq. Control **45**(2), 431 (1998).
[17] T. Fjield, X. Fan, and K. Hynynen, ''A parametric study of the concentric-ring transducer design for MRI guided ultrasound surgery,'' J. Acoust. Soc. Am. **100**, 1220–1230 (1996).
[18] C. A. Cain and S. A. Umemura, ''Concentric-ring and sector vortex phased array applicators for ultrasound hyperthermia therapy,'' IEEE Trans. Microwave Theory Tech. **MTT-34**, 542–551 (1986).